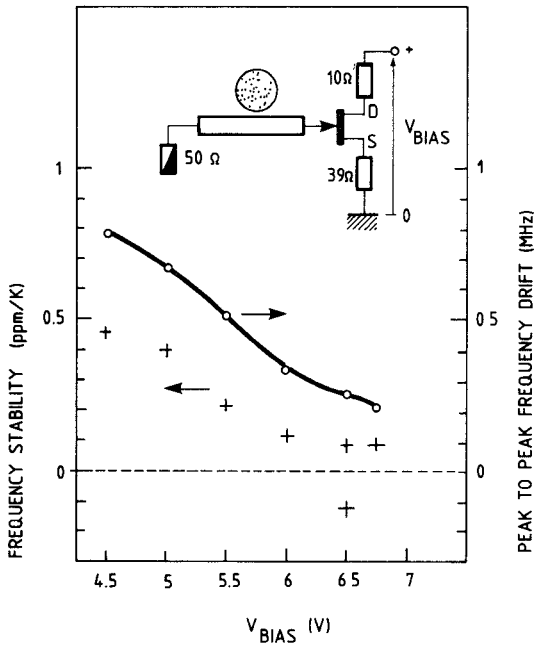

Fig. 7. Peak-to-peak frequency deviation and overall frequency slope of FET DRO using the Br 5 resonator for temperature variation between −30°C and 75°C.

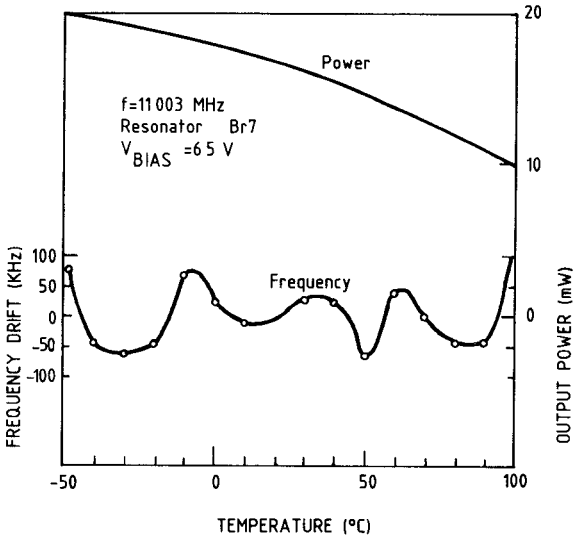

Fig. 8. Long-term frequency stability and power variation with temperature of FET DRO using the Br 7 dielectric resonator (76 mol% B_2T_9; 24 mol% BT_4).

deviation remains about ±100 kHz from −50°C to +100°C. In this case, the final positioning of the resonator was indeed more tedious than in the case of the Br 5 resonator.

Further experiments with several very stable oscillators using other dielectric materials have shown that the unavoidable long-term drift in the characteristics of the resonator and the FET in this free-running oscillator type cause at least a total frequency drift of 100 to 200 kHz over a 100 deg. temperature variation that can be considered as the natural fluctuation limit of this type of free-running oscillator.

On the other hand, the above-mentioned stabilities have been found quite reproducible when measured several times over a time period of several months.

V. Conclusion

We presented a general investigation of the stabilization procedure of GaAs FET oscillators using dielectric resonators. The influence of coupling, temperature coefficient, and quality factor of the resonators on frequency drift has been analyzed. New specifically developed homogenous materials on the basis of $Ba_2Ti_9O_{20}$ and $BaTi_4O_9$ have been tested and employed in order to realize ultra-stable DRO's. Reproducible stabilities of ±100 kHz over −50 to 100°C at 11 GHz have been achieved.

Acknowledgment

The author is grateful to J. L. Gras who carried out all oscillator and resonator measurements and A. Villegas Danies who realized the circuits. Dr. D. Hennings has developed the new dielectric material at Philips Research Laboratory, Aachen. Finally, the author acknowledges the clarifying discussions with V. Pauker and P. Lesartre at LEP.

References

[1] M. Purnell, "The dielectric resonator oscillator—A new class of microwave signal source," *Microwave J.*, pp. 103–108, Nov. 1981.
[2] H. Abe *et al.*, "A highly stabilized low-noise GaAs FET integrated oscillator with a dielectric resonator in the *C* band," *IEEE Trans. Microwave Theory Tech.*, vol. MTT-26, pp. 156–162, 1978.
[3] T. Makino and A. Hashima, "A highly stabilized MIC Gunn oscillator using a dielectric resonator," *IEEE Trans. Microwave Theory Tech.*, vol. MTT-27, pp. 633–638, 1979.
[4] Y. Komatsu *et al.*, "A frequency stabilized MIC oscillator using a newly developed dielectric resonator," in *IEEE MTT-S Symp. Dig.*, 1981, pp. 313–315..
[5] C. Tsironis and P. Lesartre, "Temperature stabilization of GaAs FET oscillators using dielectric resonators," in *Proc. 12th Eur. Microwave Conf.* (Helsinki), 1982, pp. 181–185.
[6] H W. Brand and D. Hennings, private communication.

The Annular Slot Antenna In a Lossy Biological Medium

R. D. NEVELS, MEMBER, IEEE, C. M. BUTLER, FELLOW, IEEE, AND W. YABLON, MEMBER, IEEE

***Abstract*—An integral equation is formulated for a coaxially fed annular aperture antenna. The integral equation in terms of the unknown tangential aperture electric field is solved numerically by the Method of Moments. The coaxial feed line is air filled while the exterior region consists of i) air, ii) fat or bone, and iii) muscle. Results are given for the aperture electric field, apparent input admittance, and contours of constant power absorption when the excitation frequency is 2.45 GHz.**

I. Introduction

The annular slot aperture antenna fed by a coaxial waveguide (Fig. 1) is a classic problem in electromagnetics [1]. Recently, the

Manuscript received December 12, 1983; revised November 5, 1984.
R. D. Nevels is with the Department of Electrical Engineering, Texas A&M University, College Station, TX 77843.
C. M. Butler is with the Department of Electrical Engineering, University of Houston, Houston, TX 77004.
W. Yablon is with Nurad, 2165 Druid Park, Baltimore, MD 21211.

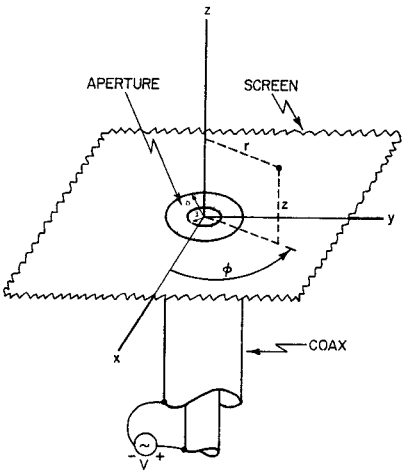

Fig. 1. Annular slot antenna fed by a coaxial waveguide with an inside radius a and outside radius b.

use of microwave hyperthermia for cancer treatment has produced a resurgence in interest in the coaxial aperture antenna. In the past, authors have addressed the problems of finding the input admittance and the far and intermediate radiated fields. The medium external to the coaxial feed line has most often been assumed to be air or at least lossless and homogeneous. Biological materials, however, are lossy, and researchers are more interested in the near radiated field since this is the region in which most of the power is deposited. It is therefore necessary to perform a more complete analysis if the input admittance and near-zone power deposition patterns are to be found.

Both the coaxial probe opening into a ground plane (noninvasive) and extending into biological tissue [2], [3] (invasive) type radiators have been studied. In order to simplify the analytical problems involved in calculating the radiated fields and input impedance, the invasive-type probe is often approximated by using the noninvasive configuration shown in Fig. 1. Measurements conducted by Bahl and Stuchly [4] indicate that this is a reasonable approximation since tissue heating produced by currents traveling on the outside coaxial sleeve appear to be small.

One of the problems associated with open-ended coaxial radiators in biological applications is that for useful sizes and frequency ranges it is difficult to match the input impedance at the open end to the characteristic impedance of the feed line. Chang [5] and Irzinski [6] have shown that if the region outside the coaxial probe is nonconducting, then under limiting conditions such a high excitation frequency where the aperture $(b-a)$ is on the order of one-half wavelength a good impedance match can be obtained. For cases where a significant mismatch occurs, simply increasing the input power at the generator has raised concern that local hot spots in the tissue may result. The issue of where hot spots will occur and how they may be prevented is currently a primary topic of research in cancer hyperthermia.

In the following section, an integral equation is formulated in terms of the unknown annular aperture tangential electric field. The integral equation is solved numerically by the Method of Moments [7]. Once the tangential aperture field is known then, by uniqueness, all the fields on both sides of the aperture can be found. Results are given for the aperture field, input admittance, and radiated near-field power patterns for selected cases where the external medium is muscle or fat and bone and the excitation frequency is 2.45 GHz. The assumed time dependence is $\exp(j\omega t)$.

II. Integral Equation Formulation

In the coaxial region, the electric and magnetic fields which satisfy the scalar homogeneous Helmholtz wave equation are

$$H_\phi(r,z) = b_0(z)\frac{1}{r} + \sum_{p=1}^{\infty} b_p(z)\frac{d}{dr}\Phi_p(r) \tag{1}$$

$$E_r(r,z) = c_0(z)\frac{1}{r} + \sum_{p=1}^{\infty} c_p(z)\frac{d}{dr}\Phi_p(r) \tag{2}$$

where the derivative of the eigenfunction $\Phi_p(r)$ is

$$\frac{d}{dr}\Phi_p(r) = -\lambda_n\left[N_0(\lambda_p a)J_1(\lambda_p r) - J_0(\lambda_p a)N_1(\lambda_p r)\right]. \tag{3}$$

The eigenvalues λ_p are the roots of

$$J_0(\lambda_p b)N_0(\lambda_p a) - J_0(\lambda_p a)N_0(\lambda_p b) = 0 \tag{4}$$

with J_n, N_n, respectively, the nth-order Bessel functions of the first and second kind. By making use of Maxwell's equations and the orthogonality properties for series and for the solutions to Bessel's equation, relationships between the coefficients in (1) and (2) are found to be as follows:

$$c_0(z) = \frac{j}{\omega\epsilon}\frac{d}{dz}b_0(z) \tag{5}$$

$$c_p(z) = \frac{j}{\omega\epsilon}\frac{d}{dz}b_p(z) \tag{6}$$

$$b_0(z) = B_0^+ e^{-jkz} + B_0^- e^{+jkz} \tag{7}$$

$$b_p(z) = B_n^- e^{\alpha_p z} \tag{8}$$

where the propagation constants α_p are

$$\alpha_p = \begin{cases} \sqrt{\lambda_p^2 - k^2}, & \lambda_p^2 > k^2 \\ j\sqrt{k^2 - \lambda_p^2}, & \lambda_p^2 < k^2 \end{cases}. \tag{9}$$

The permeability, permittivity, and propagation constants in the coaxial line are defined, respectively, by μ, ϵ, and $k = \omega(\mu\epsilon)^{1/2}$.

The coefficients in (5)–(8) are found by the procedure described below. Equations (5)–(8) are substituted into (2), which yields

$$E_r(r,z) = \frac{\eta}{r}\left[B_0^+ e^{-jkz} - B_0^- e^{+jkz}\right] + \frac{j}{\omega\epsilon}\sum_{p=1}^{\infty}\alpha_p B_n^- e^{\alpha_p z}\frac{d}{dz}\Phi_p(r). \tag{10}$$

We assume that the coaxial waveguide is excited by a TEM wave given by

$$E_r^i = \frac{V}{\ln\frac{b}{a}}\cdot\frac{1}{r}e^{-jkz} \tag{11}$$

where V is the incident voltage amplitude. The TEM mode of excitation assumption does not necessarily restrict the approach in the derivation of the interior fields. However, the coefficients below are different if the coaxial line is excited by a higher order mode. Since the total electric field traveling in the $+z$ direction in the coaxial line is given by (11), then the coefficient B_0^+ in (10) must be

$$B_0^+ = \frac{1}{\eta}\cdot\frac{V}{\ln\frac{b}{a}} \tag{12}$$

where $\eta = (\mu/\epsilon)^{1/2}$ is the intrinsic wave impedance. Orthogonality conditions are applied to (10) in order to determine the remaining coefficients

$$B_0^- = \frac{1}{\eta \ln \frac{b}{a}} \left[V - \int_{r=a}^{b} E_r^a(r)\, dr \right] \tag{13}$$

$$B_p^- = -\frac{j\omega\epsilon}{\alpha_p M_p^2} \int_{r=a}^{b} r E_r^a(r) \frac{d\Phi_p(r)}{dr} \tag{14}$$

where $E_r^a(r) = E_r(r,0)$ is the electric field in the aperture, and

$$M_p^2 = -\frac{2}{\pi^2} + \lambda_p^2 \frac{b^2}{2} \left[N_0(\lambda_p a) J_1(\lambda_p b) - J_0(\lambda_p a) N_1(\lambda_p b) \right]^2. \tag{15}$$

The interior magnetic field is now completely determined in terms of the aperture electric field $E_r^a(r)$. The coefficients (12)–(14) are substituted into (1) thus yielding

$$H_\phi(r,z) = \frac{V}{\eta \ln \frac{b}{a}} \cdot \frac{1}{r} \left\{ e^{-jkz} + \left[1 - \frac{1}{V} \int_{r'=a}^{b} E_r^a(r')\, dr' \right] e^{jkz} \right\}$$

$$- j\omega\epsilon \sum_{p=1}^{\infty} \frac{e^{\alpha_p z}}{\alpha_p M^2} \left(\int_{r'=a}^{b} r' E_r^a(r') \frac{d}{dr'} \Phi_p(r')\, dr' \right) \frac{d}{dr} \Phi_p(r). \tag{16}$$

The equivalence principle of electromagnetics [8] is applied in order to find an expression for the exterior magnetic field. First, the aperture is short-circuited and magnetic currents which maintain the original radiating fields are placed over the region bounded by the shorted aperture. The method of images are then used, resulting in an equivalent annular magnetic current

$$M_\phi = -2E_r^a(r) \tag{17}$$

which radiates into free space. The magnetic field valid on and above the conducting ground plane is therefore

$$H_\phi^+(r,z) = \frac{j\omega\epsilon_+}{2\pi} \int_{r'=a}^{b} r' E_r^a(r') \int_{\phi'=-\pi}^{\pi} \cos\phi' \cdot \frac{e^{-jk_+[z^2+r^2+r'^2-2rr'\cos\phi']^{1/2}}}{\left[z^2 + r^2 + r'^2 - 2rr'\cos\phi' \right]^{1/2}} d\phi'\, dr' \tag{18}$$

where k_+, ϵ_+ are, respectively, the complex propagation on dielectric constants in the exterior region. Continuity of the magnetic field through the aperture is enforced (requiring that (16) and (18) be equal at $z = 0$) to obtain

$$\frac{1}{\eta \ln \frac{b}{a}} \cdot \frac{1}{r} \int_{r'=a}^{b} E_r^a(r')\, dr'$$

$$+ j\omega\epsilon \sum_{p=1}^{\infty} \frac{1}{\alpha_p M_p^2} \left(\int_{r'=a}^{b} r' E_r^a(r') \frac{d}{dr'} \Phi_p(r')\, dr' \right) \frac{d}{dr} \Phi_p(r)$$

$$+ \frac{j\omega\epsilon_+}{2\pi} \int_{r'=a}^{b} r' E_r^a(r') \int_{\phi'=-\pi}^{\pi} \cos\phi' \frac{e^{-jk_+R}}{R} d\phi'\, dr' = 2 \frac{V}{\eta \ln \frac{b}{a}} \cdot \frac{1}{r} \tag{19}$$

where

$$R = \left[r^2 + r'^2 - 2rr'\cos\phi' \right]^{1/2}. \tag{20}$$

The first term in (19) represents that portion of the incident TEM wave which is reflected back along the coaxial line. The second term represents the higher order modes which are produced by the aperture discontinuity and travel back long the coaxial line. The third term represents the field radiated by the annular aperture, and the term on the right-hand side of (19) represents the coaxial line TEM mode excitation.

III. Reflection Coefficient and Apparent Input Admittance

In coaxial lines of practical interest and which support only the TEM mode, higher order modes produced by the aperture become negligible at a distance of a few wavelengths from the aperture. In (16), the infinite sum which represents the higher order modes can therefore be dropped when the field is evaluated at a significant distance from the aperture. From (16), the TEM reflection coefficient, which is the ratio of incident and reflected fields, is therefore determined to be

$$\Gamma_{\text{in}}(z) = -\left(1 - \frac{1}{V} \int_{r'=a}^{b} E_r^a(r')\, dr' \right) e^{j2kz}. \tag{21}$$

The input admittance as a function of position z is

$$Y(z) = Y_0 \left(\frac{1 - \Gamma_{\text{in}}(z)}{1 + \Gamma_{\text{in}}(z)} \right) \tag{22}$$

where Y_0 is the coaxial line characteristic admittance $Y_0 = 2\pi/\eta \ln(b/a)$. By allowing z to approach 0, we obtain the apparent aperture admittance

$$Y^a = Y_0 \left[\frac{2}{\frac{1}{V} \int_{r'=a}^{b} E_r^a(r')\, dr'} - 1 \right]. \tag{23}$$

It is interesting to anticipate tests which can be performed with the aid of (23) in order to determine the numerical accuracy of $E_r^a(r)$. If the coaxial line is matched, then $\int_a^b E_r(r)\, dr$ should be equal to the incident voltage amplitude V in the aperture. In that case, the expected result given by (23) is $Y^a = Y_0$. A second test can be performed by noting that an ideal transmission-line open circuit is obtained when $b - a \ll \lambda$. At an ideal open circuit, the voltage doubles so that one would expect that $\int_a^b E_r^a(r)\, dr = 2\ V$. From (23), if E_r^a is calculated under the $b - a \ll \lambda$ condition, then the expected value $Y^a = 0$ should result.

IV. Numerical Method

The Method of Moments [6] procedure is used to solve the integral equation (19). The fact that the aperture field is ϕ-independent led us to choose a subdomain basis function which is a set of concentric rings each of width Δr. The aperture tangential electric field is therefore expanded as

$$E_r^a(r) = \begin{cases} \dfrac{V_n}{r}, & r\epsilon(r_n - \Delta r/2, r_n + \Delta r/2) \\ 0, & \text{otherwise} \end{cases}. \tag{24}$$

Since the basis functions in (24) form concentric rings which vary as $1/r$ in the aperture, a simplification of the integrals in (19) occurs. In fact, the first two integrals in (19) can be evaluated analytically, which results in a significant reduction in computer computation time. Delta testing functions T_m are used where

$$T_m = \delta(r - r_m), \qquad m = 1,2,\cdots,N$$

so that match points occur at the radial direction centers of the basis function rings.

Equation (24) is substituted into (19) and the symmetric product is taken with the testing functions T_m, thereby yielding the matrix equation

$$[Y_{mn}][V_n] = [I_m] \tag{25}$$

where

$$Y_{mn} = \frac{\ln\left(\frac{r_n + \Delta r}{r_n - \Delta r}\right)}{\eta \ln\left(\frac{b}{a}\right)} + j\omega\epsilon r_m \sum_{p=1}^{\infty} \frac{1}{\alpha_p M_p^2}\left[\Phi_p(r_n + \Delta r/2) - \Phi_p(r_n + \Delta r/2)\right] + \frac{j\omega\epsilon_+ r_m}{2\pi} \int_{r'=r_n-\Delta r}^{r_n+\Delta r} \int_{\phi=-\pi}^{\pi} \cos\phi' \frac{e^{-jk_+R}}{R}\, d\phi'\, dr'$$

with

$$R = \left[r_m^2 + r'^2 - 2r_m r' \cos\phi'\right]^{1/2} \tag{26}$$

and

$$I_m = \frac{2V}{\eta \ln\frac{b}{a}}. \tag{27}$$

The admittance matrix in (25) is inverted and multiplied by the current vector $[I_m]$. The voltage vector result when substituted into (24) gives the tangential aperture electric field.

V. Power

Power radiated by the aperture is obtained by calculating both the electric and magnetic near fields. The electric field is found from

$$\boldsymbol{E} = -\frac{1}{\epsilon_+} \nabla \times \boldsymbol{F} = \left(-\frac{1}{\epsilon_+}\frac{\partial F_\phi}{\partial \rho} + \frac{1}{\rho} F_\phi\right)\hat{z} \tag{28}$$

where

$$F_\phi = -\frac{\epsilon_+}{2\pi} \int_a^b r' E_r^a(r') \int_{-\pi}^{\pi} \cos(\phi') \frac{e^{-jk_+R}}{R}\, d\phi'\, dr' \tag{29}$$

and

$$R = \left[r^2 + r'^2 - 2rr'\cos\phi' + (z - z')^2\right]^{1/2}. \tag{30}$$

By substituting (29) and the numerical approximation for the aperture electric field given by (24) into (28) one gets [9]

$$\boldsymbol{E} = -\frac{1}{2\pi} \sum_{n=1}^{N} V_n \left\{ \int_{\phi'=0}^{2\pi} \frac{e^{-jk_+R}}{R}\bigg|_{r_n-\Delta/2}^{r_n+\Delta/2} d\phi'\,\hat{z} + \int_{r_n-\Delta/2}^{r_n+\Delta/2} \int_{\phi'=0}^{2\pi} z\cos\phi' \left[\frac{jk_+}{R^2} + \frac{1}{R^3}\right] d\phi'\, dr'\,\hat{r} \right\}. \tag{31}$$

The magnetic field is

$$\boldsymbol{H} = -j\omega F_\phi \hat{\phi} \tag{32}$$

which, upon substituting (24) into (29), becomes

$$H_\phi = \frac{jk_+}{2\pi\eta_+} \sum_{n=1}^{N} V_n \int_{r'=r_n-\Delta/2}^{r_n+\Delta/2} \int_{\phi'=0}^{\pi} \cos(\phi') \frac{e^{-jk_+R}}{R}\, d\phi'\, dr' \tag{33}$$

where η_+ is the complex intrinsic wave impedance in the exterior region.

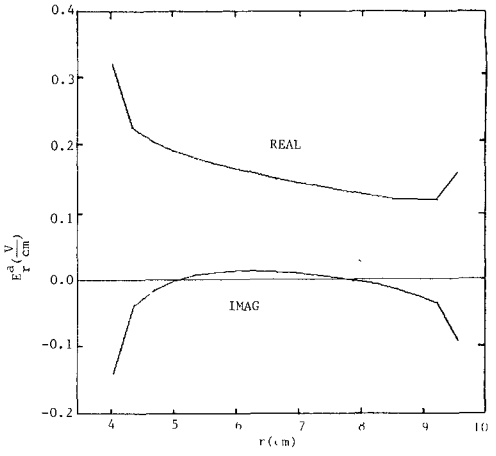

Fig. 2. Real and imaginary parts of annular aperture electric field when the exterior region is free space, $b/a = 2.5$, and $ka = 2.0$.

Equations (31) and (33) are substituted into the time average Poynting vector

$$\boldsymbol{S} = \frac{1}{2}\,\mathrm{Re}[\boldsymbol{E} \times \boldsymbol{H}^*] \tag{34}$$

in order to determine the magnitude and direction of power flow in the medium above the coaxial aperture.

VI. Results and Conclusions

Fig. 2 shows the tangential aperture electric field for an air-filled coaxial line opening into a free-space air region. The $1/r$ variation in the field through the center of the aperture illustrates the behavior of the dominant TEM mode. The edge condition which is supplied by the higher order modes appears to be satisfied near $r = a, b$. In Section III, two methods for checking the accuracy of the numerically determined aperture electric field are described. These tests involving ideal transmission-line open-circuit and matched-load conditions were carried out and the predicted results were obtained in each case.

A comparison has been made between the apparent input admittance calculated as described above and the measured results previously reported by Levine and Papas [1]. The comparison which is shown in Fig. 3 is very favorable and indistinguishable from the results of an analytical approach reported by Irzinski [6]. It should be noted that it would be very difficult to obtain a general analytical solution if the exterior region were lossy.

It is easier to understand the coaxial aperture antenna if the input admittance is plotted on a Smith Chart. Fig. 4 shows a Smith Chart plot of the input admittance from the data given in Fig. 3. It can be seen that for low excitation frequencies ($b - a \ll \lambda$) the aperture behaves like an ideal open circuit. However, as the frequency is increased, the aperture has the nature of a lossy capacitor. At certain frequencies, the input admittance approaches the center of the Smith Chart, a point at which the transmission line becomes matched to free space.

The input admittance as a function of ka is shown in Fig. 5 for an air-filled coax with an excitation frequency of 2.45 GHz and exterior regions consisting of fat or bone ($\epsilon = 4.51 - j\ 0.843$) and muscle ($\epsilon = 49.61 - j\ 16.52$). In each case, we obtained input admittance data first with only the TEM incident and reflected modes in the coax, and then the higher order modes were added to the reflected field. Regardless of whether higher order modes are considered or not, it is found that for the fat or bone and muscle cases the input admittance was virtually the same. In fact,

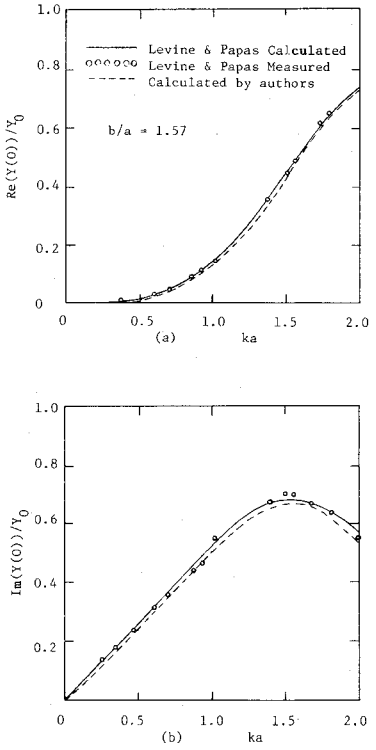

Fig. 3. Apparent normalized input admittance comparison between the calculated and measured results of Levine and Papas and the calculated results obtained by the authors.

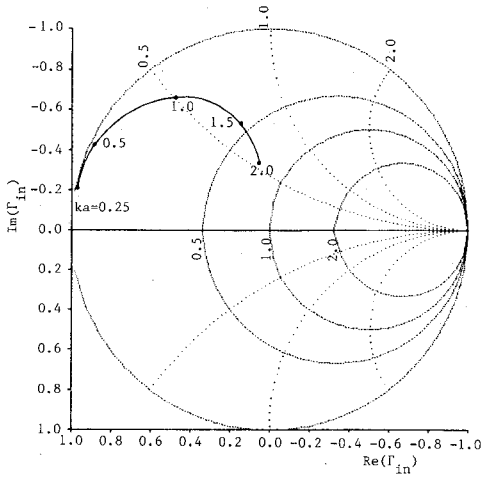

Fig. 4. Smith Chart plot of the apparent input admittance as a function of ka when the exterior region is free space and $b/a = 1.57$.

the numerical difference was in the third significant figure. Although input admittance data was obtained for many b/a ratios, we found that it is not possible to obtain a wide aperture plus an impedance match when the exterior medium is muscle. However, when the exterior medium is fat or bone, a value of $ka \doteq 1.3$ gives a VSWR less than 2.0 for almost all ratios of $b/a < 2.5$. This point is illustrated in two cases ($b/a = 1.25$ and $b/a = 1.5$) for fat and bone shown in Fig. 5.

In order to determine the actual temperature in tissue as a function of time, one must solve the bio-heat equation [10]. However, under steady-state conditions, the power absorption distribution calculated from $\sigma|E|^2$ is approximately proportional to the temperature distribution in the tissue. Fig. 6 shows two

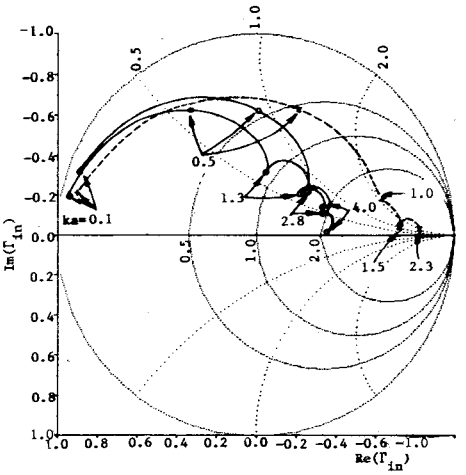

Fig. 5. Apparent input admittance at 2.45 GHz when the exterior region is composed of fat or bone $\epsilon = 4.51 - j\ 0.843$ with $b/a = 1.25$ (—●—●—), $b/a = 1.5$ (—○—○—), and muscle $\epsilon = 49.61 - j\ 16.52$ with $b/a = 1.25$ (--x--x--).

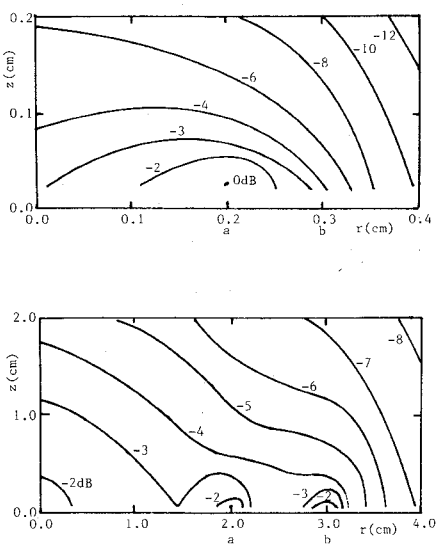

Fig. 6. Power deposition patterns at 2.45 GHz when the exterior region is composed of fat or bone ($\epsilon = 4.51 - j\ 0.843$), $b/a = 1.5$, and (a) $ka = 0.1$, (b) $ka = 1.0$.

examples of power absorption patterns: in Fig. 6(a), $(b - a) \ll \lambda$ and in Fig. 6(b), $(b - a)$ is an appreciable portion of a wavelength. In each case, the greatest power absorption is in the aperture plane near the inside edge ($r = a$) of the center conductor. However, in the wider aperture case, a large amount of power is also absorbed around $r = 0$ and $r = b$ in the aperture plane.

If one were to attempt to heat a large region of tissue using the open-ended probe described here, then burn areas also referred to as "hot spots" are likely to occur at points of high power absorption. At least one "hot spot" will occur for any set of aperture dimensional parameters. We have therefore concluded that an open-ended probe should not be used for hyperthermia applications.

As an academic exercise, it is interesting to plot the direction and magnitude of the time average power flux density flowing through the coaxial aperture for various a to b ratios. One such case is shown in Fig. 7. Power seems to flow from the aperture in much the same way water sprays from a hose nozzle. The largest power flow amplitude in the aperture occurs near the radius of

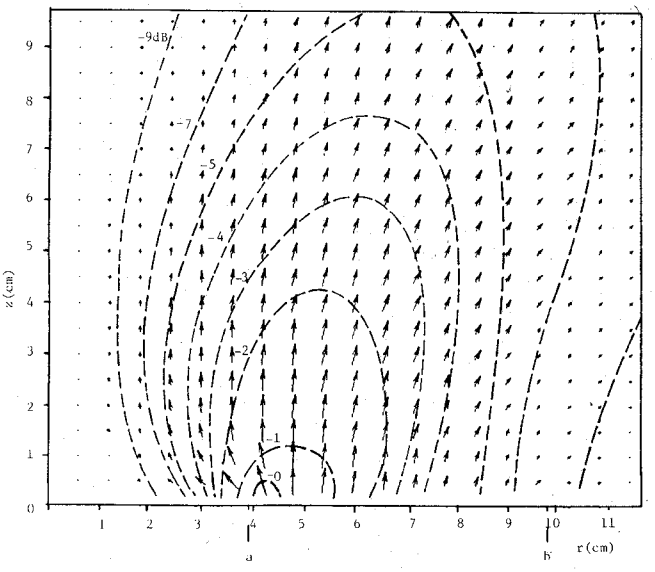

Fig. 7. Constant time-average power density patterns and power flow directions when the exterior region is air, $b/a = 2.5$, and $ka = 2.0$.

the center conductor. At distances several wavelengths from the center of the annular aperture, the power flow turns toward the radial direction. Contours of constant power flux density appear as dashed lines in Fig. 7. An expected null exists on the vertical center axis due to the interaction of fields on opposite sides of the annular ring.

The addition of higher order reflected modes has been observed to have little effect on the input admittance. Virtually no difference is observed between the input admittance results for the two approaches (with or without higher order interior modes) when the exterior region is composed of fat or bone and muscle. These are cases where, in the exterior region, the aperture size is less than 2.5 wavelengths and the medium is lossy. As long as the aperture size remains less than 2.5 wavelengths in the exterior medium, the lack of an effect by the higher order modes on the input admittance tends to support previous work [11] which relies solely on TEM modes to determine the dielectric constant of materials in the exterior region.

References

[1] H. Levine and C. H. Papas, "Theory of the circular diffraction antenna," *J. Appl. Phys.*, vol. 22, pp. 29–43, Jan. 1951.
[2] L. S. Taylor, "Electromagnetic syringe," *IEEE Trans. Bio-med. Eng.*, vol. BME-25, pp. 308–309, May 1978.
[3] M. L. Swicord and C. C. Davis, "Energy absorption from small radiating coaxial probes in lossy media," *IEEE Trans. Microwave Theory Tech.*, vol. MTT-29, pp. 1202–1209, Nov. 1981.
[4] I. J. Bahl and S. S. Stuchy, "The effect of finite size of the ground plane on the impedance of a monopole immersed in a lossy medium," *Electron. Lett.*, vol. 15, pp. 728–729, 1979.
[5] D. C. Chang, "Input admittance and complete near-field distribution of an annular aperture antenna driven by a coaxial line," *IEEE Trans. Antennas Propagat.*, vol. AP-18, pp. 610–616, Sept. 1970.
[6] E. P. Irzinski, "The input admittance of a TEM excited annular slot antenna," *IEEE Trans. Antennas Propagat.*, vol. AP-23, pp. 829–834, Nov. 1975.
[7] R. Harrington, *Field Computation by the Method of Moments*. New York: Macmillan, 1968.
[8] R. Harrington, *Time Harmonic Electromagnetic Fields*. New York: McGraw-Hill, 1961, ch. 3.
[9] C. M. Butler and L. L. Tsai, "An alternate frill field formulation," *IEEE Trans. Antennas Propagat.*, vol. AP-21, pp. 115–116, Jan. 1973.
[10] A. W. Guy, J. E. Lehmann, and J. B. Stonebridge, "Therapeutic applications of electromagnetic power," *Proc. IEEE*, vol. 62, pp. 55–75, Jan. 1974.
[11] E. C. Burdette, F. L. Cain, and J. Seals, "*In vivo* probe measurement technique for determining dielectric properties at VHF through microwave frequencies," *IEEE Trans. Microwave Theory Tech.*, vol. MTT-28, pp. 414–427, Apr. 1980.

Mathematical Expression of the Loading Characteristics of Microwave Oscillators and Injection-Locking Characteristics

KATSUMI FUKUMOTO, MASAMITSU NAKAJIMA, MEMBER, IEEE, AND JUN-ICHI IKENOUE

***Abstract*—Most of the studies concerning microwave oscillators have so far been based on the Van der Pol oscillator model. However, this model is too simple to obtain good agreement between observation and theory. Our previous paper proposed a new mathematical model which describes the loading characteristics of oscillators more accurately than the Van der Pol model does. In this paper, we have investigated injection-locked microwave oscillators using the mathematical model to find out the relation between the loading and injection-locking characteristics.**

I. Introduction

Many researchers have studied the loading characteristics and locking phenomena of oscillators in the low-frequency region, in which an oscillator circuit can be treated as a lumped-constant circuit [1]. In the microwave region, however, an oscillator circuit should be treated as a distributed-constant circuit. Although there is no essential difference in the oscillation phenomena between the two frequency regions [2], the characteristics of the oscillators appear to be different between the two regions. This is mainly because, in the case of injection-locking phenomena, the input and output signals are measured in terms of voltage or current in the low-frequency region, while in the microwave region, they are measured in terms of traveling waves. The differential equations which describe the relation between the input and output signals should be practically different between the two regions. However, when the magnitude of the input signal is small, the differential equations which describe the phase relation happen to be of the same form [3]. Distinction becomes apparent when the input signal is large, the differential equations assuming different forms. Obviously, it may be reasonable to treat microwave oscillators in terms of traveling waves.

In this paper, we will analyze large-signal injection-locking phenomena using the extended oscillator model with the concept of traveling waves. We will find out the relationship between the loading characteristics and the injection-locking characteristics of oscillators. This will give us an estimate of the validity of the numerical expression of oscillator characteristics, and the usefulness of the oscillator model will be demonstrated.

The theory is confirmed to be in good agreement with experiment.

Manuscript received January 4, 1984; revised October 30, 1984.

K. Fukumoto is with the Semiconductor Research Laboratories, Sharp Corporation, Tenri, Nara, Japan.
M. Nakajima and J. Ikenoue are with the Department of Electronics, Kyoto University, Kyoto, Japan.

0018-9480/85/0400-0319$01.00 ©1985 IEEE